*Journal of Alloys and Compounds, 194* (1993) 407–415
*JALCOM 7223*



# Intrinsic response of crystals to pure dilatation*

Jinghan Wang and Sidney Yip
*Department of Nuclear Engineering, Massachussetts Institute of Technology, Cambridge, MA 02139 (USA)*
Simon Phillpot and Dieter Wolf
*Materials Science Division, Argonne National Laboratory, Argonne, IL 60439 (USA)*

(Received March 26, 1992; in final form September 14, 1992)

**Abstract**

The response of an f.c.c. lattice with Lennard-Jones interaction under symmetric lattice extension has been studied by Monte Carlo simulation at several temperatures. The critical strain at which the crystal undergoes a structural change is found to be well predicted by the mechanical stability limit expressed in terms of either the elastic constants or the bulk modulus. At low temperature (reduced temperature $T=0.125$), lattice decohesion is observed in the form of cleavage fracture, whereas at higher temperature ($T=0.3$) the strained system deforms by cavitation with some degree of local plasticity. At still higher temperature ($T=0.5$) the lattice undergoes homogeneous disordering with all the attendant characteristics of melting.

## 1. Introduction

It is by now well established that solid state amorphization (SSA), the process of crystal-to-glass transition, can be induced in intermetallic compounds by various perturbations ranging from particle beam irradiations, chemical reactions, to mechanical deformations [1–3]. A fundamental question which still remains concerns the underlying nature of the transition and the relative importance of the effects of point defects, chemical disorder, and other possible driving forces for lattice destabilization. Following the observation that structural disordering in all cases is accompanied by a volume expansion [2], it has been suggested that the role of local density variations in SSA may be analogous to that in the melting transition [4]. The implication is that at temperatures below the triple point, essentially the melting point $T_m$ at zero pressure, a sudden volume expansion (on a time scale short compared with that required for equilibrium sublimation) may bring about structural disordering.

In this paper we report the results of Monte Carlo simulation of the structural response of an f.c.c. crystal to pure dilatation imposed at constant temperatures. The purpose of the study is to test the prediction of lattice instability based on elastic constant criteria and to determine by direct observation whether crystal disordering can be induced by symmetric lattice extension. Using the Lennard-Jones potential to model the interatomic interaction, we find that the critical strain at which structural change occurs is well predicted by the mechanical stability limits. At low temperature (reduced temperature $T=0.125$) anisotropic lattice decohesion occurs at the critical strain and overall the system remains crystalline. At higher temperature ($T=0.3$) cavitation-like local deformation occurs with indications of anisotropic disordering. At still higher temperature ($T=0.5$) the lattice disorders uniformly with all the characteristics of melting.

## 2. Simulation model and procedure

The simulation system is a cubic cell of $N$ particles arranged on an f.c.c. lattice. The particles interact with each other through a Lennard-Jones (6–12) potential which is truncated at a distance $R_c$ and shifted to zero at the cut-off. The cell is periodic in all three directions. In each simulation run at a certain temperature, the lattice parameter $a$ is held fixed while the particles are allowed to move by a Monte Carlo process [5]. The process is then repeated at an incrementally larger $a$. Typically the first 10000 moves per particle are discarded as equilibration, and another 30000 moves per particle are made to accumulate the configurations for property calculations. All quantities reported below will be ex-

*Paper presented at the Symposium on Solid State Amorphizing Transformations, TMS Fall Meeting, Cincinnati, OH, October 21–24, 1991.

0925-8388/93/$6.00

pressed in reduced units where length and energy are scaled by the parameters $\sigma$ and $\epsilon$ of the potential.

Simulation of strain-induced response has been carried out at the temperatures $T=0.125$, 0.3, 0.5, and 0.8. (As a reference, for the Lennard-Jones potential $T_m$ can be taken to be 0.61 [6].) Most of the runs were made with a cell of 500 particles, but runs using $N=108$ and 864 were also performed to give some indications of system size effects. In all the runs the value of $R_c$ is 2.3273.

## 3. Pressure and potential energy responses

Figure 1 shows the variation at $T=0.3$ of the hydrostatic pressure, calculated using the virial expression [7], as the lattice parameter $a$ of the f.c.c. cell is increased incrementally. Starting at a value of the lattice parameter which gives zero pressure, the system is seen to go into negative pressure as isotropic strain is imposed. This negative pressure increases monotonically and appears to level off at a maximum value. With further lattice dilatation the pressure first decreases somewhat and then jumps abruptly to a considerably reduced though still finite value. The $N=500$ data exhibit this characteristic behavior quite clearly. The data for $N=864$ are quite consistent with these results, whereas the onset of the abrupt change in the small system, $N=108$, occurs at a somewhat larger value of strain.

Figure 2 shows the potential energy of the system in response to isotropic strain. As the lattice goes into negative pressure, more and more strain energy is stored in the system. This continues until the pressure changes suddenly (*cf.* Fig. 1), at which point the potential energy

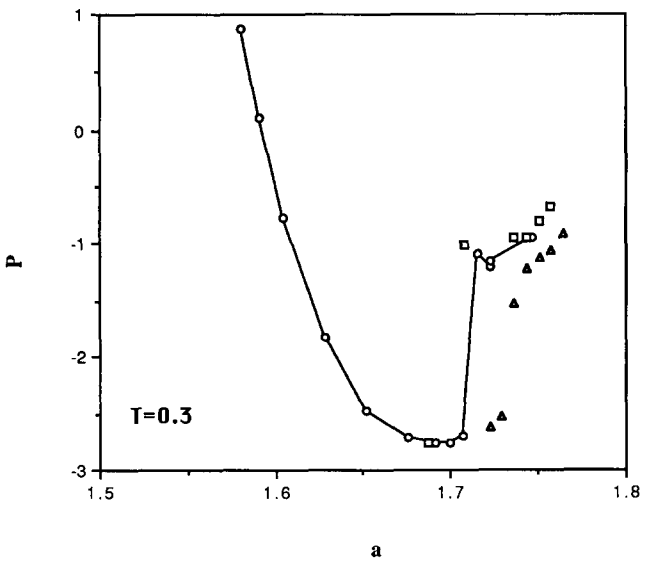


Fig. 1. Variation in hydrostatic pressure with lattice parameter $a$ at $T=0.3$: $N=108$ (△), 500 (○), 864 (□).

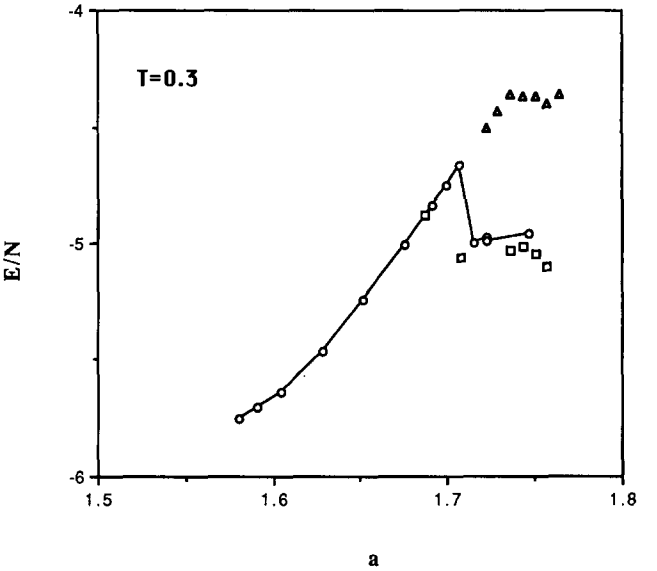


Fig. 2. Same as Fig. 1 except variation is that of the potential energy.

drops correspondingly. Again, the $N=864$ data are consistent with the $N=500$ results, whereas for $N=108$ the decrease in potential energy occurs at higher strain and is barely discernible.

The existence of a critical value of imposed strain, as indicated in Figs. 1 and 2, suggests the onset of a structural transition which we will investigate in the following by examining directly the atomic configurations produced at each incremental strain. As for the nature of the transition, one can ask what the connection is between the behavior observed in Fig. 1 and the mechanical stability limit which one can derive for a uniform lattice. We have already noted that the tension appears to reach a maximum value at a lattice parameter which we will denote by $a_c$, and that $a_c$ is distinctly smaller than the critical value at which the pressure jumps suddenly, which we will denote by $a_p$. Since we have results for three system sizes, we can perform a $1/N$ extrapolation on the value of $a_p$ as directly observed in the simulation data. This gives a critical strain $\epsilon_p=(a_p-a_0)/a_0=0.0687$. To determine $\epsilon_c$, we fit for each $N$ the several data points for the pressure in the vicinity of $a_c$ to a polynomial, and calculate $dp/da=0$ from the fit. After a similar $1/N$ extrapolation we obtain $\epsilon_c=0.0628$. The apparent discrepancy between $\epsilon_p$ and $\epsilon_c$ is believed not to be significant given the large fluctuations in the system pressure in the region of the critical behavior, and the fact that system size effects may not have been fully eliminated in our $1/N$ extrapolation based on limited data.

## 4. Elastic constants

Returning to the question of intrinsic mechanical stability limit, we have determined the elastic constants

of a cubic lattice by applying the fluctuation formula derived by Ray *et al.* [8] for a stressed solid. In the case of uniform strain, the adiabatic elastic constant $C_{ijkl}$ is given by

$$C_{ijkl} = \frac{l_0}{l}\left[ -\frac{V}{k_B T}\delta(P_{ij}P_{kl}) + \frac{2Nk_B T}{V}(\delta_{il}\delta_{jk}+\delta_{ik}\delta_{jl}) + \frac{1}{V}\langle \sum_{b>a} f(r_{ab})x_{abi}x_{abj}x_{abk}x_{abl}\rangle \right] \quad (1)$$

where

$$f(r) = r^{-2}[\mathrm{d}^2u(r)/\mathrm{d}r^2 - \chi(r)] \quad (2)$$

$$P_{ij} = \frac{1}{V}\left[ \sum_a p_{ai}p_{aj}/m - \sum_{b>a}\chi(r_{ab})x_{abi}x_{abj} \right] \quad (3)$$

and $\chi(r) = [\mathrm{d}u(r)/\mathrm{d}r]/r$, with $u(r)$ being the interatomic potential function. In eqn. (1) $l_0$ and $l$ are the lengths of the simulation cell before and after respectively the imposed strain, $V$ is the volume of the strained cell which contains $N$ particles, and $\langle\rangle$ denotes an ensemble average. In addition, $r_{ab}$ is the separation distance between particles $a$ and $b$, and $x_{abi}$ is the $i$th cartesian component of the vector $r_{ab}$. In eqn. (3), $p_{ai}$ is a momentum component and $m$ the particle mass, and thus $P_{ij}$ is the stress tensor.

Applying eqn. (1) to the atomic configurations generated by the Monte Carlo runs, we have computed the three elastic constants $C_{11}$, $C_{12}$, and $C_{44}$. For a lattice to be mechanically stable one can show that the inequalities

$$C_{11} > 0,\ C_{11} - C_{12} > 0,\ C_{44} > 0 \quad (4)$$

must hold [9], together with $C_{12} > 0$, arising from the physical condition that the Poisson ratio must be greater than zero [10]. These criteria may be compared with the requirement of positive isothermal bulk modulus $B_T = -V(\partial P/\partial V)_T$, a thermodynamic condition. Our elastic constant results at $T = 0.3$ and different system sizes are shown in Fig. 3. It can be seen that all three elastic constants have decreased to quite small values in the region of the critical strain. The elastic constants behave normally while they are still positive, but, once an elastic constant has reached zero value, subsequent behavior at still larger strain displays unphysical oscillations. The first term in eqn. (1) represents the effects of stress tensor fluctuations. In the critical-strain region it is large and fluctuates strongly, thus giving rise to appreciable uncertainties in the calculated elastic constants. As a result we can only say that, as $C_{11}$ approaches $C_{12}$, both appear to be approaching zero. At the same time, the data suggest that $C_{44}$ remains finite at the critical strain. Within the estimated statistical error the mechanical stability limit seems to be consistent with $\epsilon_c$.

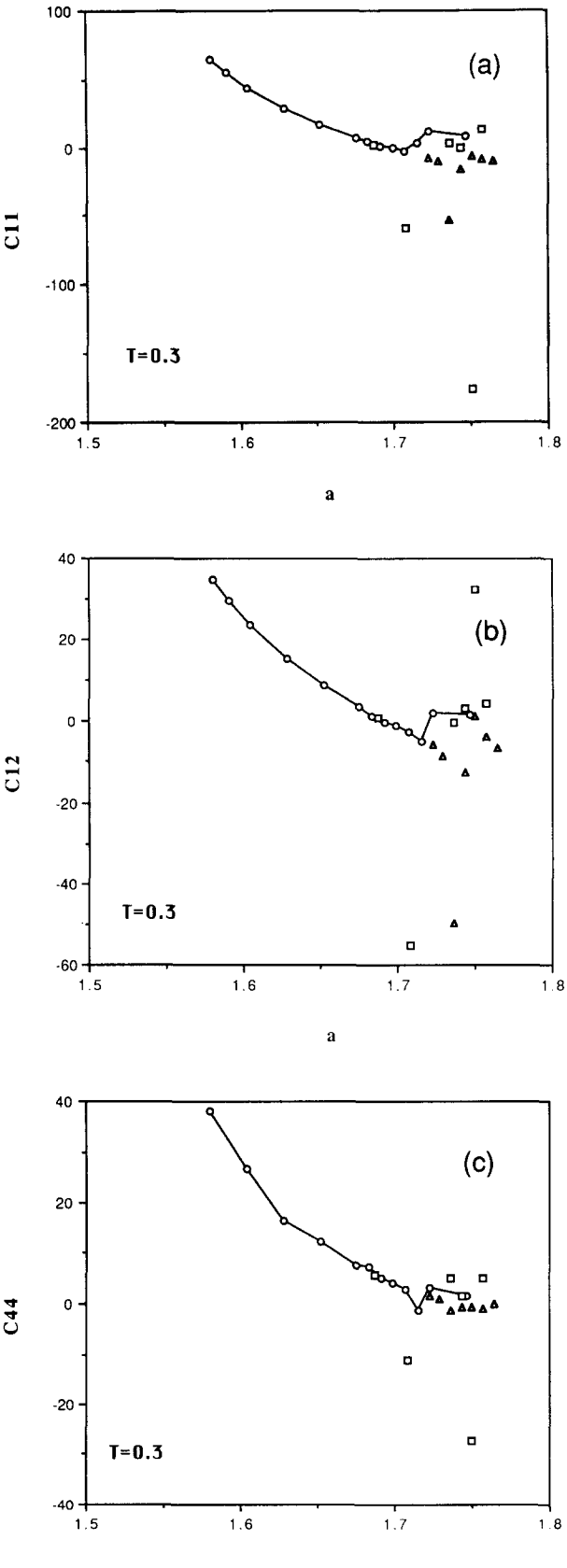


Fig. 3. Variations in the elastic constants (a) $C_{11}$, (b) $C_{12}$, and (c) $C_{44}$ with lattice parameter $a$ at $T = 0.3$: $N = 108$ (△), 500 (○), 864 (□).

## 5. Structural responses

The onset of a sudden change in the pressure and potential energy is an indication that an accompanying structural change must have also occurred. The above consideration of mechanical stability, while useful for determining the critical strain at which this change takes place, tells us nothing about the state into which the system evolves. For this information it is necessary to examine the atomic configurations at various stages of strain.

We will characterize the atomic configurations in terms of the radial distribution function $g(r)$ [7] which provides a measure of local spatial correlation, without specification of direction, and the corresponding quantity the static structure factor $S(\boldsymbol{k})$, with $\boldsymbol{k}$ being a wavevector. By computing $S(\boldsymbol{k})$ for a large number of suitably chosen $\boldsymbol{k}$, one can generate a diffraction pattern which provides a measure of direction-dependent structural order in the system.

Figure 4 shows the $g(r)$ and $S(\boldsymbol{k})$ results for the $T=0.3$ runs with $N=500$ at three values of the lattice parameter $a$: $a=a_1=1.707$ specifies the system strain just before the pressure jump (*cf.* Fig. 1), $a=a_2=1.723$ is the value after two strain increments, and $a=a_3=1.747$ is the last dilatation imposed in this series. First we notice that in all three cases the $g(r)$ results are quite similar; in particular, a distinct peak can be seen at $r\approx 1.7$, the characteristic second-neighbor shell of the

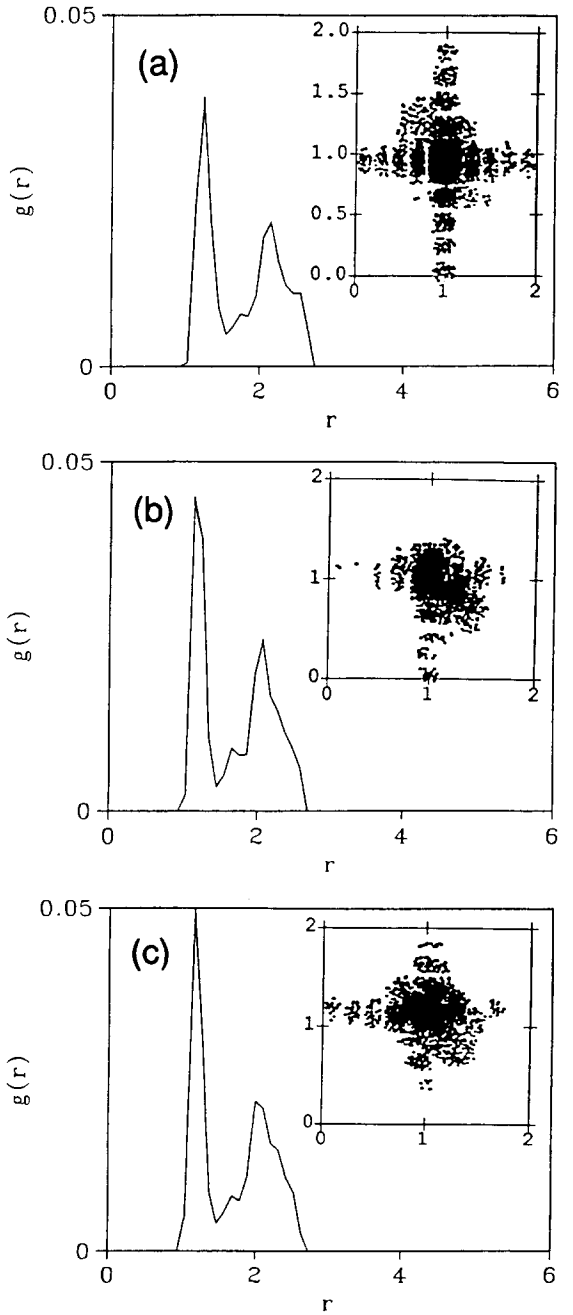


Fig. 4. System responses $g(r)$ and diffraction pattern $S(\boldsymbol{k})$ at $T=0.3$, $N=500$, and three values of the lattice parameter: (a) $a=1.707$, (b) $a=1.723$, and (c) $a=1.747$. $S(\boldsymbol{k})$ is shown in each part as projections on $k_x$ (horizontal axis) and $k_y$ (vertical axis).

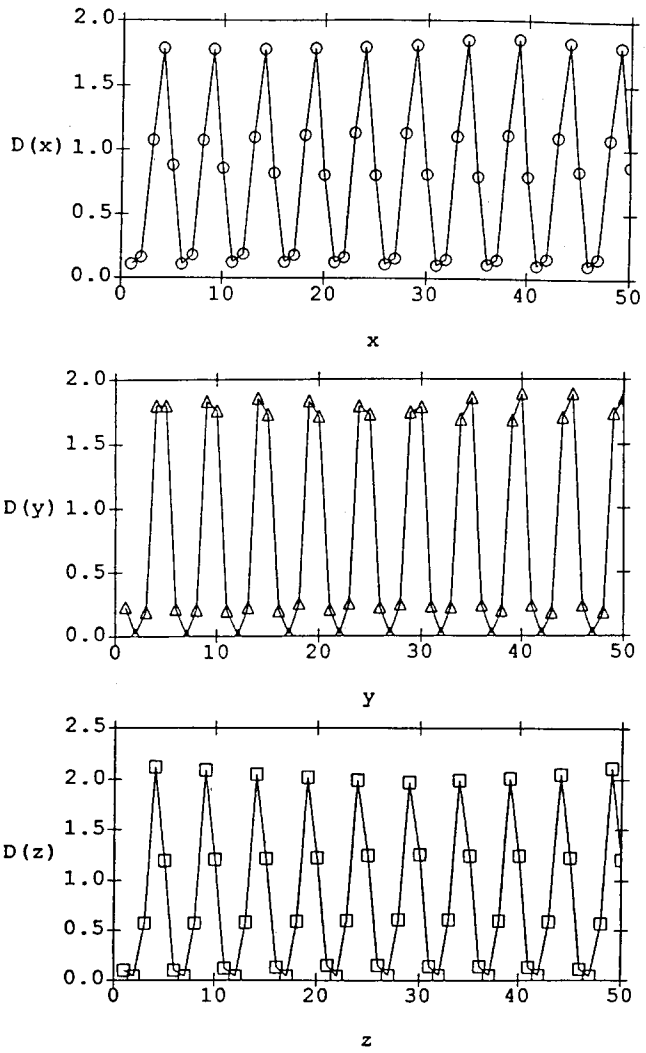


Fig. 5. Density profiles corresponding to Fig. 4(a).

f.c.c. lattice. The corresponding diffraction patterns all display high intensity in the region around $k_x \approx k_y \approx 1$, as one would expect for the f.c.c. lattice. However, whereas the diffraction pattern at $a_1$ is quite symmetric, an asymmetry along $k_x$ and $k_y$ about the Bragg position $k_x = k_y = 1$ can be noticed at $a_2$ and $a_3$.

More detailed information on the structural change in going from $a_1$ to $a_2$ and $a_3$ is provided by the density profiles given in Figs. 5–7. One sees that at $a_1$ the atomic planes along each direction of cubic symmetry are well ordered as in a perfect (undeformed) lattice. At $a_2$, after the pressure jump, symmetry is clearly broken in the $y$ direction; there appears an extra atomic plane along this direction, and, moreover, the system is no longer uniform along this direction. Another feature that can be seen in Fig. 6 is the distinctly non-zero value of the minima in the density profiles which implies significant atomic displacements from the original lattice positions. In going from $a_2$ to $a_3$ (Fig. 7) the density profile along the $y$ direction displays two extra planes relative to the $x$ and $z$ directions. We interpret this as a tendency to change from cubic to tetragonal structure. Also, the non-uniform density profiles along the $x$ and $y$ directions suggest the nucleation of cavitation, first seen in Fig. 6 along the $y$ direction.

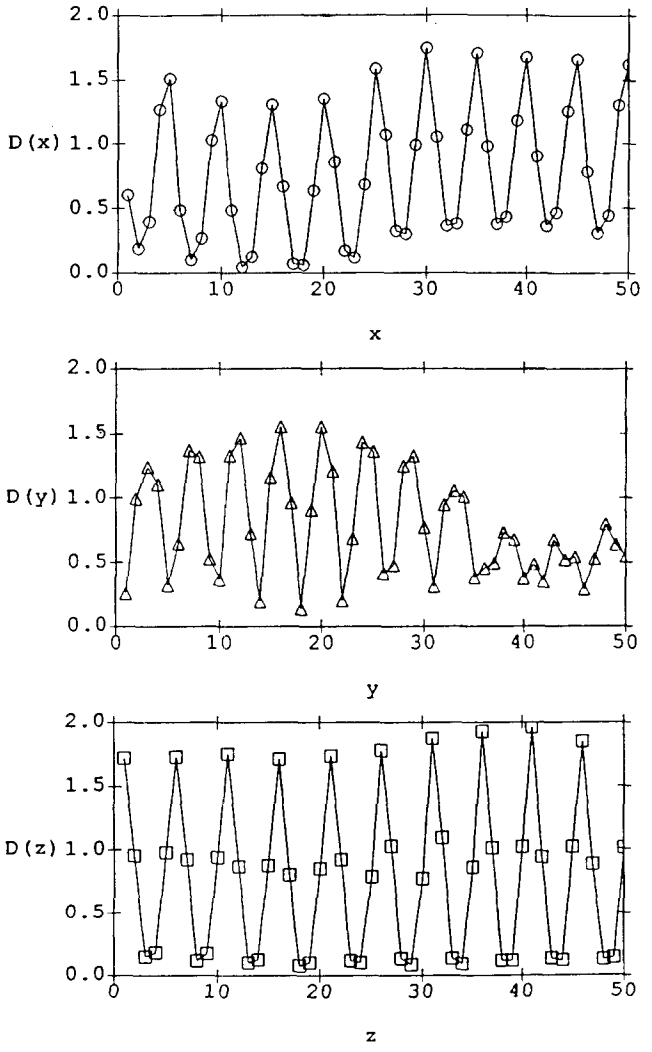


Fig. 6. Density profiles corresponding to Fig. 4(b).

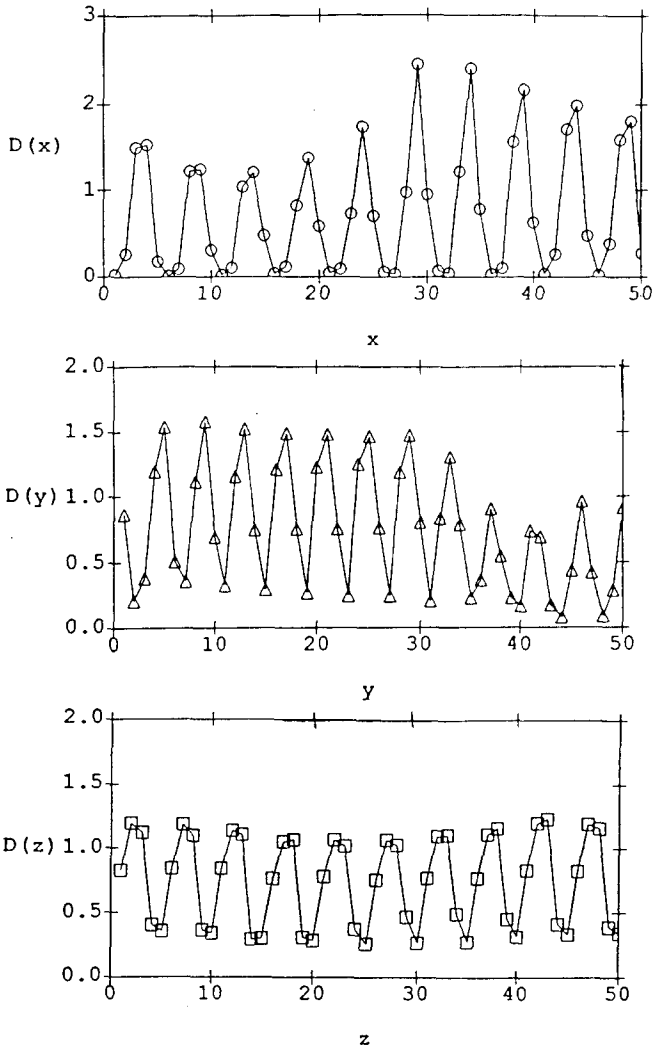


Fig. 7. Density profiles corresponding to Fig. 4(c).

One may ask whether further structural changes will take place if the dilatation were increased further. In the series of simulations at $T = 0.3$ using the $N = 864$ system, we have taken the system out to larger values of lattice parameter as shown in Fig. 8. Up to approximately the same value of $a = a_3$, the observed behavior is similar to the $N = 500$ data shown in Figs. 4–7. When the imposed strain is increased to $a_4 = 1.750$ and $a_5 = 1.757$, the density profiles, given in Figs. 9 and 10, reveal (i) pronounced cavitation along the direction of broken symmetry ($x$ direction in this $N = 864$ series in contrast to $y$ direction in the $N = 500$ series), and (ii) increasing loss of well-ordered planar structure along the cubic directions of the original lattice. It is interesting that the structural deformations which are

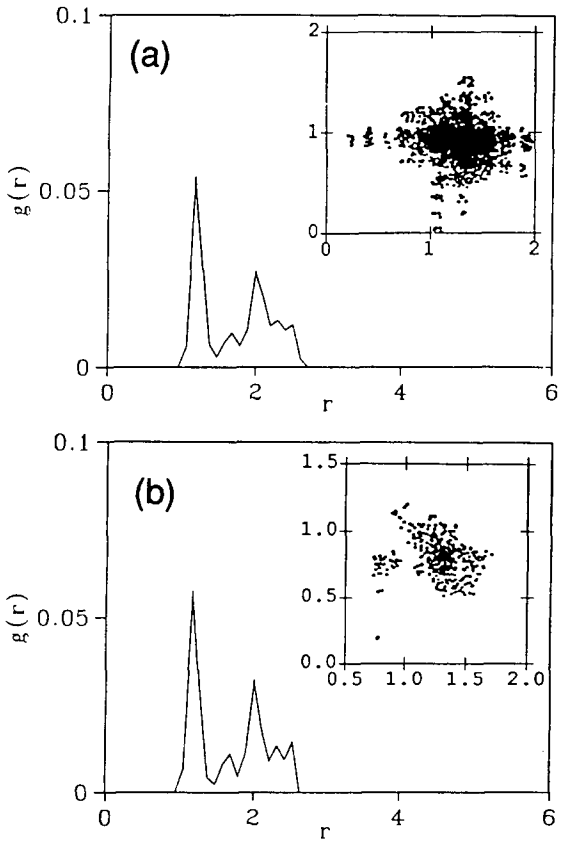


Fig. 8. Same as Fig. 4 except $N=864$ and the two lattice parameter values are (a) $a=1.750$ and (b) $a=1.757$.

clearly indicated by the density profiles do not give rise to any characteristic features in the $g(r)$ and $S(k)$ results in Fig. 8, apart from an indication of asymmetry in the latter.

The structural responses at $T=0.125$ generally are similar to those just presented at $T=0.3$. The pressure and potential energy responses exhibit the same jump behavior as in Figs. 1 and 2. The onset of cavitation is quite clearly seen and, as the system is further dilated, decohesion of the lattice planes occurs along a broken-symmetry direction.

The structural response at $T=0.5$, on the contrary, is quite different from that at $T=0.3$. Figure 11 shows a pressure jump at the critical strain, but now the corresponding potential energy change is an increase instead of a decrease as in Fig. 2. Examination of $g(r)$, $S(k)$ and density profiles at the strain after the pressure jump shows clearly that the system has become completely disordered. It is also noteworthy that the mean-squared displacement function evaluated at the strain before and after the pressure jump, given in Fig. 12, reveals dramatically different mobility behavior over the same number of Monte Carlo sweeps. The essentially linear variation in the mean-squared displacement and the increased magnitude of this quantity observed after the jump are strong indications of a liquid-like environment.

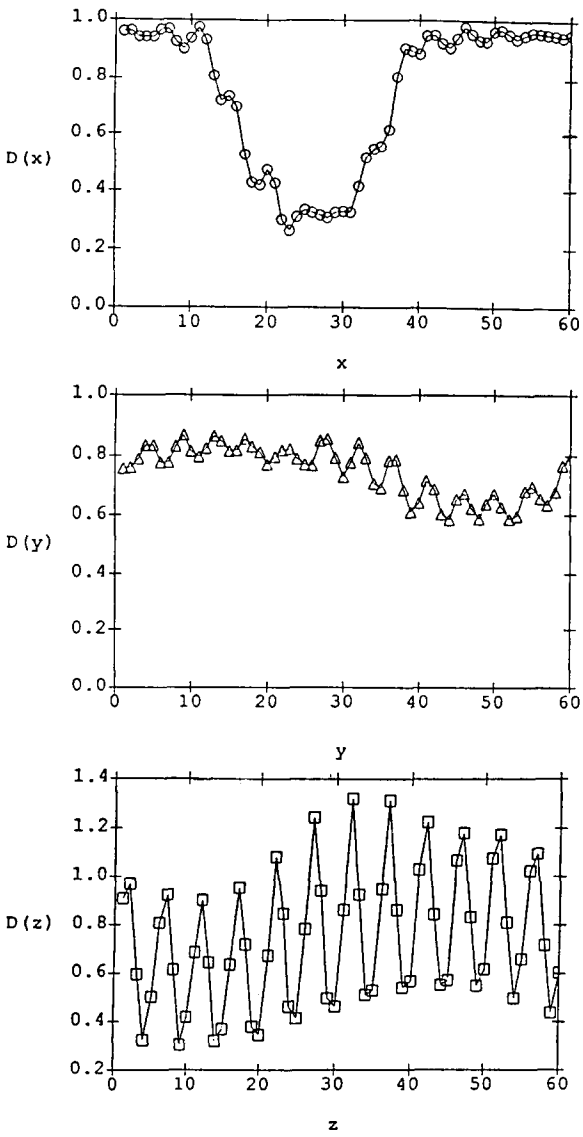


Fig. 9. Density profiles corresponding to Fig. 8(a).

## 6. Discussion

In this work we have determined by Monte Carlo simulation and elastic constant calculations the structural stability limit of an f.c.c. Lennard-Jones lattice under symmetric isothermal extension along the three directions of initial cubic symmetry. We have shown that at several temperatures the critical strain is determined by the Born criteria involving the elastic constants. The values of these strains define a stability curve in the temperature–density phase diagram as shown in Fig. 13. It has been suggested that the freezing curve which, like the melting curve, is defined only for temperatures above the triple point $T_t$, is effectively

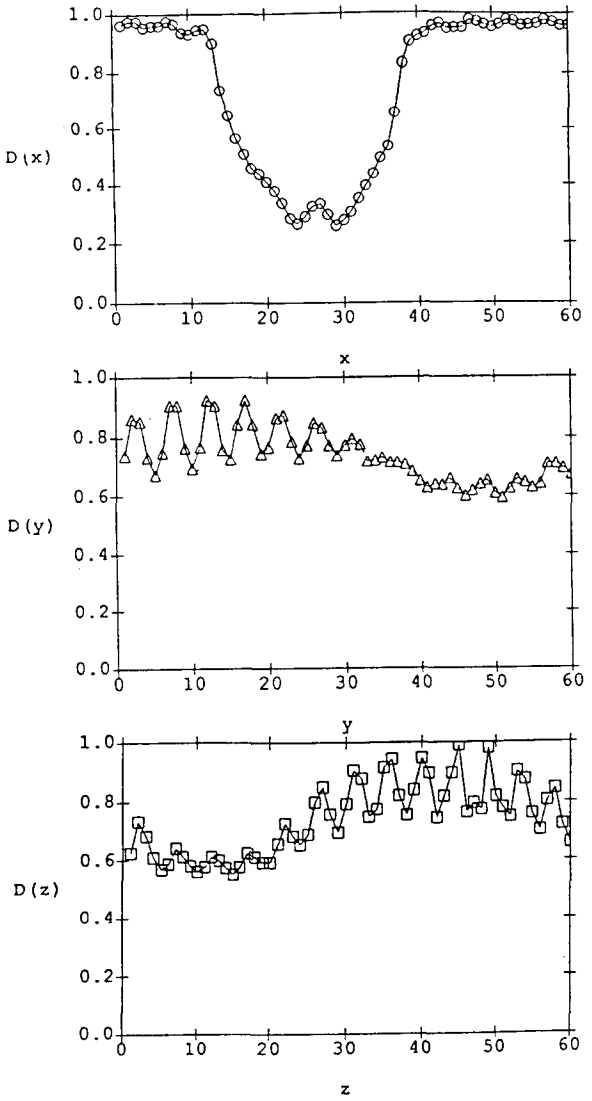


Fig. 10. Density profiles corresponding to Fig. 8(b).

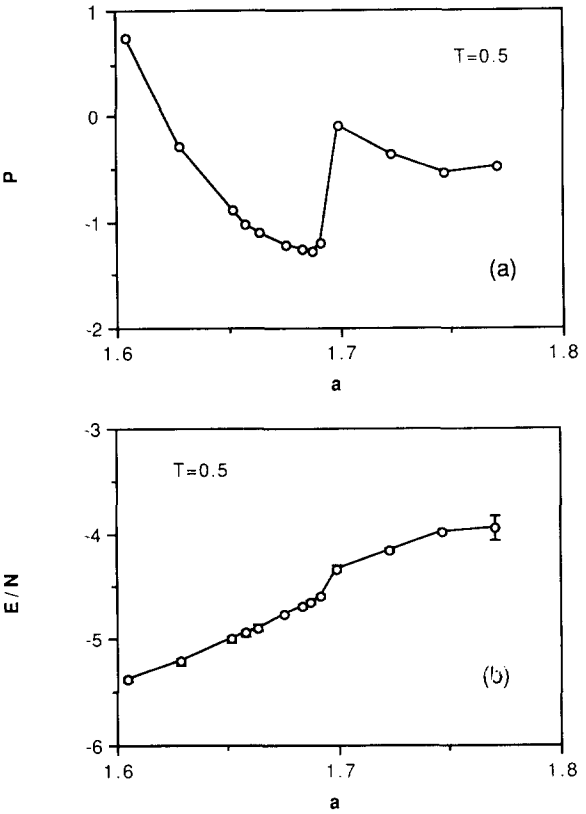


Fig. 11. System responses at $T=0.5$ and $N=500$: (a) pressure and (b) potential energy. Note similarity with Fig. 1 in the pressure and difference from Fig. 2 in the potential energy.

also the mechanical stability curve in the sense of heating a crystal rapidly up to the limit of superheating [4]. It can be seen in Fig. 13 that the critical strains observed in the present work delineate the extension of the mechanical stability curve to temperatures below $T_t$. It has been conjectured that in crossing this stability curve the lattice will become disordered, thus providing a simple thermodynamic connection between melting and SSA [4]. What we have found is that in crossing such a curve the lattice does become mechanically unstable as manifested by sudden jumps in the hydrostatic pressure and the potential energy; however, the atomic configuration into which it evolves depends on the temperature. The instability is accompanied by symmetry breaking as shown clearly by the density profiles along the three cubic directions. At the same time, the system becomes non-uniform by the formation of a local region of relatively low density. We interpret this crystal response as cavitation which at $T=0.125$ $(0.18T_t)$ leads to cleavage fracture on further lattice dilatation. At $T=0.3$ $(0.44T_t)$, in addition to cavitation-like behavior, significant local disordering occurs as the system is strained beyond the instability. At $T=0.5$ $(0.74T_t)$ the system response at the instability is homogeneous and complete disordering as in a melting transition.

Regarding the question of whether pure volume expansion is sufficient to give rise to a crystal-to-amorphous transition, it appears that the present results on the Lennard-Jones system do not give a definitive answer. We feel that part of the problem stems from the relatively shallow well depth of the potential as compared with an EAM-type potential [12] for metals. Thus the Lennard-Jones potential gives considerably lower values for the elastic constants which make it difficult to distinguish between the criteria given by eqn. (4) and $C_{12}>0$. A study is underway using an EAM potential for f.c.c. metals to see the influence of potential function details on the structural response to imposed strain.

As far as equation of state behavior is concerned, we can compare the Lennard-Jones system with the universal binding energy model [13], a simple two-parameter empirical description of the variation in the cohesive energy (the potential energy at zero temper-

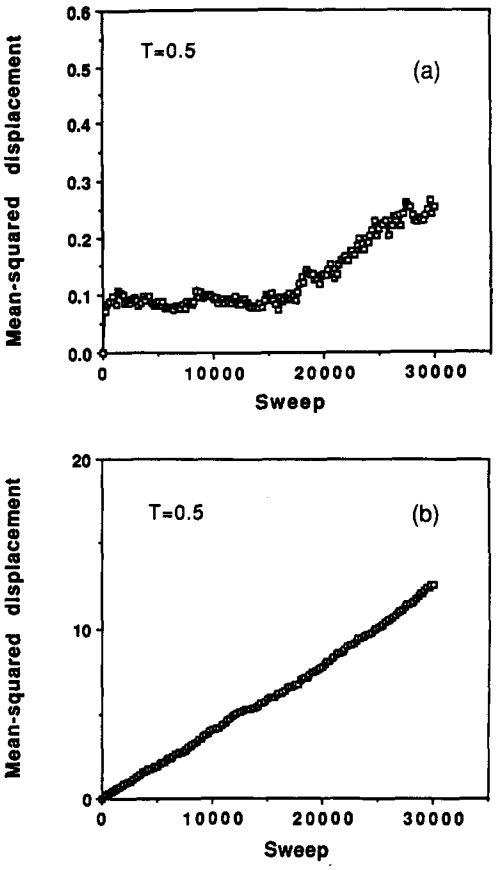


Fig. 12. Variation in mean-squared displacement function with number of Monte Carlo sweeps at two system strain states, (a) just before and (b) just after the pressure jump shown in Fig. 11. The difference in scale of the ordinate should be noted.

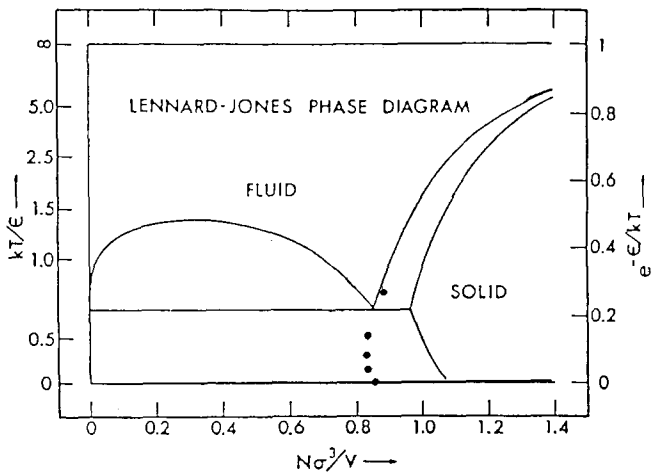


Fig. 13. Temperature–volume phase diagram of an atomic system in which the particles interact via the Lennard-Jones potential function [11]. Critical strains, converted to densities, observed in the present simulation are added at the various temperatures (●).

ature) with lattice parameter. According to this model, $E(a)=\Delta E\ E^*(a^*)$, with

$$E^*(a^*)=-(1+a^*+0.05a^{*3})e^{-a^*} \quad (5)$$

where $\Delta E$ is the minimum value of the cohesive energy and $a^*=(a-a_E)/l$, $a_E$ being the lattice parameter at which the cohesive energy is a minimum and $l$ a length scale which can be determined from the bulk modulus [13]. $E^*$ and $a^*$ are the scaled energy and lattice parameter. Figure 14(a) shows the comparison between the Lennard-Jones result and eqn. (5). Given $E(a)$ one can find the pressure at zero temperature from $P=-\mathrm{d}E/\mathrm{d}V$:

$$P(V)=3B[(V/V_0)^{1/3}-1](V/V_0)^{-2/3} \times(1-0.15a^*+0.05a^*)e^{-a^*} \quad (6)$$

where $B$ is the bulk modulus and $V_0=4\pi a_E^3/3$. The comparison of the pressure calculated directly for the Lennard-Jones lattice with eqn. (6) is shown in Fig. 14(b). Taken together with Fig. 14(a) these results show how well the Lennard-Jones system can be described by the simple analytic expressions given by the universal binding energy model, a description which has been found useful for metals. To see the effects of temperature we show in Fig. 15 the pressure variation in the vicinity of the critical strain obtained from the Monte Carlo

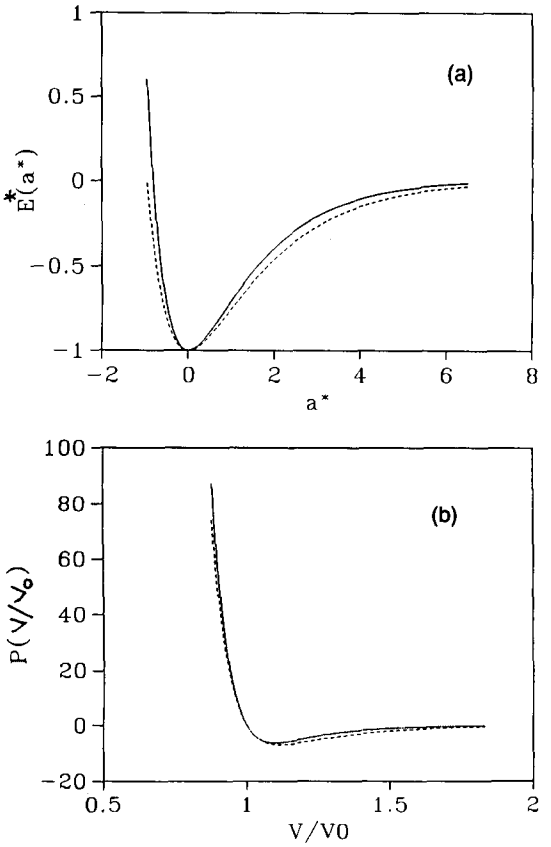


Fig. 14. Comparison of (a) the cohesive energy and (b) the pressure–volume relation of the Lennard-Jones crystal at zero temperature (——) with the universal binding energy model (– – – –). Procedure used in scaling the lattice parameter and energy is discussed in the text.

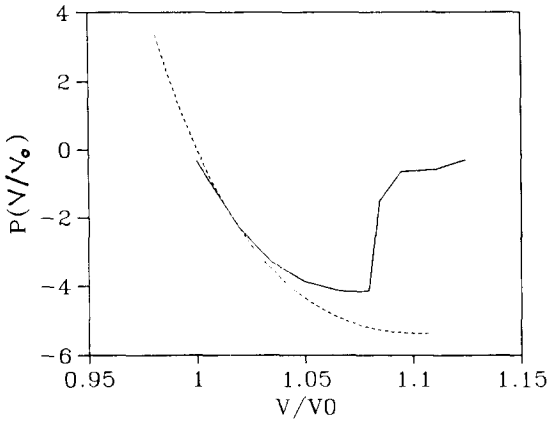


Fig. 15. Pressure–volume relation of the Lennard-Jones crystal at $T=0.125$ (——) showing a jump which is absent in the universal binding energy model (– – – –, same result as in Fig. 14 but on a different scale).

simulation at $T=0.125$ and the zero-temperature variation given by eqn. (6). The absence of a pressure jump in the latter clearly underscores the role of thermal fluctuations in symmetry breaking and initiation of structural deformation.

## Acknowledgments

Work of J. W. and S. Y. has been supported in part by a National Science Foundation Grant CHE-8806767, and by the Materials Science Division at the Argonne National Laboratory. Work of S.P. and D.W. was supported by the US Department of Energy BES–Materials Science under Contract W-31-109-Eng-38. Support for computational resources also has been provided by an allocation from the San Diego Supercomputer Center.

## References

1 W. L. Johnson, *Prog. Mater. Sci., 30* (1986) 81.
D. E. Luzzi and M. Meshii, *Res. Mech., 21* (1987) 207. *J. Less-Common Met., 140* (1988).
2 P. R. Okamoto and M. Meshii, in H. Wiedersich and M. Meshii (eds.), *Science of Advanced Materials*, ASM International, Materials Park, OH, 1990, p. 33.
3 W. L. Johnson, in D. Wolf and S. Yip (eds.), *Materials Interfaces – Atomic-Level Structure and Properties*, Chapman and Hall, London, 1992, p. 516.
4 D. Wolf, P. R. Okamoto, S. Yip, J. F. Lutsko and M. Kluge, *J. Mater. Res., 5* (1990) 286.
5 N. Metropolis, A. W. Rosenbluth, M. N. Rosenbluth, A. H. Teller and E. Teller, *J. Chem. Phys., 21* (1953) 1087.
6 J. Q. Broughton and G. H. Gilmer, *J. Chem. Phys., 79* (1983) 5095.
7 M. P. Allen and D. J. Tildesley, *Computer Simulation of Liquids*, Clarendon, Oxford, 1987.
8 J. R. Ray, M. C. Moody and A. Rahman, *Phys. Rev. B, 32* (1985) 733.
9 M. Born, *Proc. Cambridge Philos. Soc., 36* (1940) 160.
F. Milstein and R. Hill, *Phys. Rev. Lett., 43* (1979) 1411.
10 L. D. Landau and E. M. Lifshitz, *Theory of Elasticity*, Pergamon, Oxford, 1959, p. 14.
11 W. G. Hoover and W. T. Ashurst, in *Theoretical Chemistry – Advances and Perspectives*, Vol. 1, Academic Press, New York, 1975, p. 1.
12 M. S. Daw and M. I. Baskes, *Phys. Rev. B, 29* (1984) 6443.
13 J. H. Rose, J. R. Smith, F. Guinea and J. Ferrante, *Phys. Rev. B, 29* (1984) 2963.